# Hydrophilicity and surface heterogeneity of $TiO_2$-doped silica materials for membrane applications

Vittorio Boffa,[1] Laura Parmeggiani,[2] Asbjørn Haaning Nielsen,[3] Giuliana Magnacca,[2]*

[1]Department of Chemistry and Bioscience, Aalborg University, Fredrik Bajers Vej 7H, DK9100 Aalborg, Denmark.

[2] Universitá di Torino, Dipartimento di Chimica, NIS and INSTM Reference Centre, Via P.Giuria 7, 10125 Torino, Italy.

[3]Department of Civil Engineering, Aalborg University, Sofiendalsvej 9-11, DK9200 Aalborg SV, Denmark.

*Corresponding author:

Universitá di Torino

Dipartimento di Chimica

Via P.Giuria 7

10125 Torino, Italy.

e-mail address: giuliana.magnacca@unito.it

**Abstract**

Silica materials containing different amount of titania (namely from 0 to 33%) were prepared, characterized and tested to evaluate their hydrophilic features in order to design a good membrane material for water purification.XRD, HRTEM, nitrogen gas-volumetric adsorption at 77K were applied to obtain a complete structural and morphological description of the systems. Material stability in alkaline solutions was clearly enhanced by adding $TiO_2$ to the silica material. Adsorption microcalorimetry and microgravimetric measurements were used to study water and toluene adsorption, respectively, in order to assess the hydrophilic and hydrophobic behaviors of the materials using polar (water) and non-polar (toluene) probe molecules. Microcalorimetric data allowed to describe also the energetic features of the water adsorption giving interesting information on the microscopic environment of the adsorption sites. The analysis procedure applied in this study can constitute a valid approach to determine *a priori* the behaviors of membrane materials.

**Keywords**

Membrane material, hydrophilicity, water adsorption, microcalorimetry, chemical stability.

## 1. Introduction

Microporous and mesoporous materials with narrow pore size distribution and high pore volume are of great interest for membrane applications [1,2]. Especially materials with 1-2 nm large pores can be used as a nanofiltration layer for water softening [3] or for the removal of emerging pollutants (e.g. pharmaceuticals [4], hormones [5], and pesticides [5,6]). Thus, the development of such materials might have a high impact on water purification technologies.

Over the last twenty years, silica has been widely considered as membrane material, because microporous [7] and mesoporous [8,9] defect-free silica layers with well-defined pore structure can be fabricated by facile sol-gel coating procedures. Highly stable silica-based membranes can be obtained by introducing organic moieties in the silica network [10-12] or by inorganic doping [13]. Both approaches have been proven to be highly effective in the stabilization of silica networks. Moreover, these modifications can change porosity, pore charge density, isoelectric point, and hydrophilicity of silica network, thus impacting membrane selectivity and permeability. Hydrophilicity is an especially important feature for membrane materials, because it can strongly affect membrane permeability to water or organic solvents. Thus, developing materials with controlled hydrophilicity is of prime importance from a membrane application perspective. The hydrophilic/hydrophobic behavior of organo-modified silica membranes has been extensively investigated, as membrane affinity for non-polar solvents can be intuitively increased via the replacement of the hydrophilic surface hydroxyl groups by hydrophobic hydrocarbon chains [14]. Membrane hydrophobicity can also be tuned by covering their pore surface with alkyl groups of various lengths. “Super-hydrophobic” silica membranes have been prepared by applying long

hydrocarbon chains [15,16] or fluorinated chains [17], and highly hydrophilic membranes have been prepared by the introduction of amino groups on the pore surface [18]. Although these aspects can be very important to develop a membrane with high selectivity towards specific targets, the studies concerning truly inorganic silica membranes have been until now mainly focused on their chemical and hydrothermal stability [13,19-29], and not so much on their surface properties [27,28]. At the authors' best knowledge, change in membrane hydrophilicity upon chemical modification has been reported only for nickel-doped silica membranes, for which the hydrogen/steam selectivity was found to increase with the Ni/Si ratio, suggesting that membranes with higher Ni loading were more hydrophobic [29].

In this study, we investigate the impact of titania doping on the hydrophilicity of unsupported nanofiltration silica materials for membranes fabrication. $TiO_2$-doped silica has been selected as a suitable membrane material, because it has been shown that $TiO_2$ doping can increase the chemical and hydrothermal stability of silica membranes without a large reduction of membrane pore volume [13]. Moreover, the sol-gel method allow for the fabrication of membranes with high $TiO_2$ loading, good homogeneity and strong adhesion on the membrane support. This fabrication method consists in the use of alkoxides as precursors for the synthesis of stable nanocolloids, which are coated on a ceramic support and calcined to obtain a selective membrane layer. Finally, it was proved that $TiO_2$-doped silica can originate good membranes, since one of the formulation studied in this paper was used to fabricate a membrane which was applied with excellent results in water softening [14].

Mesoporous $TiO_2$-silica powders with different composition were prepared by the sol-gel method. Cetyltrimethylammonium bromide (CTAB) was applied as pore-

forming agent, in order to imprint similar porosity in all the materials presented in this study. After morphological investigation by XRD, TEM and low-temperature $N_2$ adsorption analysis, and tests of stability at different pHs, the hydrophilicity of the materials was determined by means of an adsorption microcalorimeter coupled with a gas-volumetric glass apparatus. This technique allows for the quantitative measure of the amount of water adsorbed as a function of water pressure admitted on the sample and the direct measurement of molar heat of adsorption of water molecules at the surface of the membrane material as a function of the surface coverage. In general, a strongly exothermic water adsorption is an indication of a highly hydrophilic surface [30-33] and the liquefaction enthalpy of water vapor (44 kJ $mol^{-1}$) can be taken as threshold reference value to classify a surface as hydrophilic (enthalpies higher than 44 kJ $mol^{-1}$) or hydrophobic (enthalpies lower than 44 kJ $mol^{-1}$) [34]. Number, strength, and strength distribution of the water adsorption sites were measured as a function of surface coverage for eight $TiO_2$-silica powders with different composition, but similar pore structure. Surface hydrophobicity was also tested for selected materials with a different technique, i.e. microgravimetry, in order to verify the gas-volumetric results obtained with water and adsorption microcalorimetry by measuring materials affinity towards a hydrophobic vapor, namely toluene. These adsorption results, coupled with morphological characterization, allowed developing understanding on the effect of $TiO_2$-doping on hydrophilicity and surface heterogeneity of silica-based membrane materials, and gave interesting insights on features of colloids specifically designed for membrane fabrication [14], allowing to obtain results suitable for further development of enhanced nanofiltration membranes.

## 2. Experimental

### 2.1 Sol synthesis

Unsupported membranes were prepared by the sol-gel method. The following reagents were used: tetraethylorthosilicate (TEOS, 99.0% Sigma Aldrich), titanium(IV) tetrabutoxide ($Ti(butO)_4$, 97%, Sigma Aldrich), ethanol (99.9% Kemityl), nitric acid (69% Sigma Aldrich), cetyltrimetylammonium bromide (CTAB, Sigma Aldrich). Since $Ti(butO)_4$ is more sensitive to hydrolysis and condensation than TEOS, the sols were prepared following a two-step synthesis method, which was designed with the aim to obtaining well-developed sols avoiding gelation or precipitation, as necessary for coating step during membrane fabrication, even at a high $TiO_2$ loading. In the first step, 1.4 N nitric acid (86 mL) was slowly dropped into a mixture of TEOS (319 g) in ethanol (276 g) under vigorous stirring. The mixture was heated at 333 K for 3 h always under stirring. After that, the mixture volume was adjusted to obtain a final 1.5 M hydrolyzed-TEOS solution, which was stored at 278 K until it was used for the preparation of the unsupported membranes.

This hydrolyzed-TEOS solution was used to prepare the $TiO_2$–doped silica sols with the reagents listed in Table 1. All the reagents were cooled at 278 K before mixing. The silica sol was diluted with ethanol (Dilution 1). Doping solutions were prepared by diluting $Ti(butO)_4$ in butanol (Dilution 2) under inert atmosphere in glove box, and then added to the diluted hydrolyzed-TEOS stirring vigorously. The final volume of the reaction mixture was further adjusted with ethanol (Dilution 3). The flask containing the mixture was heated at 333 K for 90 min always under stirring. Then, 7.00 g of CTAB were added to mixture. After stirring for 5 min to allow dissolution of the surfactant, the mixture was poured in Petri dishes, where the solvent was let to evaporate for 3 days at

room temperature to form a gel. Then, the remaining solvent was removed by drying the gels in an oven at 393 K for 2 days. The dried materials were calcined at 723 K for 3 hours at a heating/cooling rate of 2 K $min^{-1}$. The amount of reagents and solvents used are summarized in Table 1 together with the short names of the samples.

### 2.2. Material characterization

Specific surface area (*SSA*) and specific pore volume ($V_P$) of materials were determined by means of $N_2$ adsorption at liquid-nitrogen boiling point in a gas-volumetric apparatus ASAP2020 (Micromeritics, Norcross USA). Samples were outgassed at 573 K *in vacuo* (residual pressure $10^{-2}$ mbar, 1 mbar = 100 Pa) for about four hours, that is, until no gaseous species arise from them. Specific surface areas were determined using the Brunauer-Emmett-Teller (BET) model [35] and porosity was studied applying the Density Functional Theory (DFT) method using slit pores shape and small regularization [36]. The crystal structure of the materials was determined by means of a X-ray diffractometer Philips PW1830 working with a Cu-Kα source and Bragg-Brentano geometry, and $TiO_2$ crystallites domain size, was evaluated. High-resolution transmission electron microscopy (HRTEM) images were obtained on a JEOL 3010-UHR instrument (acceleration potential: 300 kV). Samples for TEM investigation were supported onto holed carbon coated copper grid by dry deposition. Water uptake and molar heats of water adsorption were evaluated by a previously reported procedure [30] on an adsorption microcalorimeter Tian-Calvet (Setaram, France) equipped with a lab-made gas-volumetric apparatus for the quantitative study of surface-water interactions. A more detailed description of the apparatus is given elsewhere [31]. In the present work, samples were outgassed (< $10^{-6}$ bar) at 298 K

before adsorption experiments. Dosed amounts of steam were sent to the sample kept at 298 K and left equilibrating. The heat released was recorded for each equilibrium steam pressure. The adsorption cycle was repeated after a 298 K outgassing of the sample under vacuum. The curves relative to the first and the second adsorption cycles showed a good overlap for all the samples, suggesting that the hydrated surface with water was in all cases fully reversible upon evacuation at 298 K. For this reason only the curve relative to the first adsorption run will be reported and discussed in the following.

Microgravimetric toluene adsorption isotherms were obtained at 298 K with microbalance apparatus (IGA002 by Hiden), contacting the powders with toluene vapours. The temperature control was guaranteed by a thermostatic water bath.

**2,3. Stability tests**

0.1g of powdered material was placed in a plastic tube together with 10 mL of Milli Q water, which was made basic or acid by adding concentrate NaOH and $HNO_3$ respectively. The samples were place on an IKA horizontal shaker and shaken (20 rpm) for three days at room temperature. After removing the powder by centrifugation at a force of 700 G for 10 minutes, the leached solutions were stored at 278 K until analysed. The silicon and titanium content of the liquid samples was quantified using inductively coupled plasma optical emission spectroscopy (ICP-OES). The measurements were performed with a dual view ICP-OES instrument operated in radial view mode (iCap 6300 Duo view, Thermo Scientific). The ICP-OES was operated with a forward power of 1.15 kW at plasma and auxiliary gas flows of 12 L $min^{-1}$ and 1.0 L $min^{-1}$, respectively. The nebulizer gas pressure was set at 0.2 MPa. The samples were introduced via a cyclonic spray chamber by means of a concentric glass nebulizer at an

uptake rate of 2.0 mL $min^{-1}$. All samples were acidified before analysis by diluting 1mL of the supernatant with 1 mL 69% $HNO_3$ of SupraPur quality (SCP Science) and 8 mL of ultra-pure water (PURELAB Ultra, Elga LabWater). The ICP-OES was calibrated against external multi-element standards. Si and Ti were measured at three wavelengths each (Si: 212.412 nm, 221.667 nm, 251.611 nm; Ti: 308.802 nm, 334.941 nm, 338.376 nm) and the average values used for further data analysis. The calibration curves were obtained from a series of matrix matched external standards (0, 0.1, 1.0, 10.0, 100.0 ppm). The standards were prepared immediately before analysis. The integration time was 15 s for wavelengths below 243 nm and 5 s for wavelengths above 243 nm. Scandium (Sc: 357.253 nm) was used as internal standard (I.S.) in all samples and standards in order to compensate the matrix effects. The concentration of the I.S. was 1 mg $L^{-1}$.

## 3. Results

### 3.1 Materials characterization

For the sake of briefness, the samples will be hereinafter referred to using the designations listed in Table 1. Sol-gel derived amorphous titanium dioxide is typically converted to the crystalline anatase phase by calcination at temperatures as low as 623 K [37]. Thus, the presence of crystallites in the $TiO_2$-silica materials after calcination at 723 K was investigated by XRD analysis. The samples with a $TiO_2$ molar concentration ≤ 5.0% (powders T_0.0, T_0.5, T_1.0, T_2.0 and T_5.0) showed the typical halo of amorphous materials: Fig. 1 reports the diffractograms observed for samples with Ti loading between 0% and 5%, for the sake of brevity. A weak and broad peak forms in the $2\theta$ range 23-26° for samples prepared with a $TiO_2$ loading of 10%

and 20% (T_10 and T_20, respectively), suggesting the presence of really small crystallites in these materials. The presence of a crystalline phase becomes clear for the samples with a $TiO_2$ loading of 33% (T_33). In this case, peaks were observed at $2\theta$ of 25.4, 38.0, 48.1, 55.2 and 63.0°. These peaks are broad, as expected for small crystallites, and are assignable to the anatase $TiO_2$ phase.

The structural features observed by XRD analysis were confirmed by the TEM micrographs. A selection of the TEM pictures taken on the $TiO_2$-silica powders is given in Fig. 2. As can be observed in Fig. 2a, T_0.0 should be highly porous amorphous materials with very small pores not organized and visible in the picture as zones of different grey gradation. This is consistent with the fabrication method: CTAB can form pores of such size [38-40] and the presence of butanol as co-solvent hampers the organization of surfactant micelles in an ordered structure. Fig. 2b shows the compositional inhomogeneity of the T_5.0 sample: in fact, a phase separation is visible since some more optically dense particles of about 10 nm of diameter, which should contain a higher concentration of Ti, stand out on the rest of the matrix. Consistently with the X-ray diffractograms, this new phase appears to be amorphous. In the samples T_10 (Fig. 2c) we can observe, instead, a few nanometer-large crystallites of anatase $TiO_2$ phase, as confirmed by the analysis of the diffraction fringes. As expected, the number of these crystallites progressively increases by increasing the $TiO_2$ loading, and as shown by Fig. 2d, the samples T_20 consists of a dispersion of a few nanometers large crystallites separated by an amorphous phase. All the micrographs show that $TiO_2$ nanoparticles, when visible, are homogenously dispersed in the amorphous matrix.

### 3.2 Pore structure

The pore structure of the powders was investigated by low temperature nitrogen adsorption measurements. As shown in Fig. 3, the sorption isotherms of the eight samples analyzed in this study have a Type I shape according to IUPAC classification [41], as typical of systems presenting only micropores and/or small mesopores. The sorption curves show that for all the samples most of the nitrogen is adsorbed at a relative pressure $p/p° < 0.2$ and a plateau is present at a higher relative pressure. However, the specific amount of nitrogen adsorbed (mmol $g^{-1}$) at the plateau is different for each sample, suggesting that the membrane materials have different specific surface area (*SSA*). *SSA* and specific pore volume ($V_p$) of the eight samples are reported as a function of the $TiO_2$ loading in Fig. 4. All the materials have *SSA* above 600 $m^2$ $g^{-1}$ and $V_p$ larger than 0.7 $cm^3$ $g^{-1}$. In general, *SSA* and $V_p$ decrease by increasing the $TiO_2$ loading, nevertheless, samples with a $TiO_2$ loading ≤ 2% show higher *SSA* and $V_p$ than the pure silica sample.

The pore size distribution (*PSD*) of the eight powders is reported in Fig. 5. All *PSD* have similar shape, showing the presence of at least two families of pores, namely micropores smaller than 1 nm and pores with size between 1 and 2.5 nm. The latter pores are consistent with the use of the CTAB [38-40], which was used as pore forming agent in the synthesis of these materials. Also in this case, the integral of the *PSD* curves, i.e. the area under the PSD curves, shows an increase of pore volume for $TiO_2$ loading from 0% to 2.0% and a progressive decline for $TiO_2$ loading from 2 % to 33 %.

### 3.3 Stability tests

Chemical stability of the membrane materials was assessed from the amount of Si and Ti leached into aqueous solution at various pH at room temperature, as determined by ICP-OES analysis, according to an already reported approach [42,43] The results of these leaching tests are reported in Fig. 6. As expected, the concentration of Si and Ti is higher in the solution at pH =13 than at pH=11 and in general at basic pH than at pH=2, owning sol-gel derived silica high solubility at pH above 8 [44]. In basic environment, the amount of dissolved material progressively decreases by increasing the $TiO_2$ loading, and Ti concentration is two orders of magnitude smaller than Si concentration. On the contrary, at pH=2 the concentration of both Si and Ti increases by increasing $TiO_2$ loading to reach a maximum for the sample T_10. Then, it progressively decreases again for samples T_20 and T_33. In order to highlight the different role of the $TiO_2$ presence on the stability of the material in basic and acidic environment, the Ti molar fraction, Ti/(Ti+Si), in the solutions at pH=2 and 13 is reported as a function of the Ti molar ratio in the starting powder in Fig. 7. At pH 13, the Ti molar fraction in the leached material is smaller than in the starting powder and in general decreases with the $TiO_2$ loading. At pH 2, the leached material has a higher Ti molar fraction than that leached at basic pH and, in most of the cases, higher than in the starting powders. The Ti molar fraction in solution increases with the $TiO_2$ loading in the stating powder up to a value of about15 % for the sample T_10 and then it remain constant also for the samples T_20 and T_33.

### 3.4 Water adsorption: surface coverage

The affinity of the $TiO_2$-silica membrane materials to water was studied by means of an adsorption microcalorimeter equipped with a gas-volumetric apparatus. The data obtained over the T_10 powder are reported in Fig. 8, as illustrative example. The water vapor pressure in the sample cell was progressively increased by sending known amounts of vapor. Thus, the amount of water adsorbed ($N_{ads}$) and the heat developed by water adsorption ($Q_{ads}$) were plotted as function of the water vapor relative pressure at the equilibrium ($p/p°_{H2O}$) in Fig. 8a and Fig. 8b, respectively. The data in Fig. 8a allowed for the calculation of the surface coverage ($\sigma$), i.e. the density of the adsorbed molecules on the surface as a function of water pressure, by the following Equation: $\sigma = N_{ads} \cdot SSA$ The water surface coverage ($\sigma_{H2O}$) was measured for all the eight silica powders. Only $p/p°_{H2O} \leq 0.15$ were considered in order to examine only the water-surface interactions due to the first layer formation, and not those due to multiple layers formation or vapor condensation. Therefore, these measurements can yield quantitative information about the density of the water adsorption sites on the surface of the membrane materials.

To stress the changes in adsorption site density and thus in water uptake due to the variation of the material composition, the water surface coverage ($\sigma_{H2O}$) at $p/p°_{H2O}$ = 0,032, 0.064, 0.096 and 0.128 ($p_{0,H2O}$ = 31.3 mbar at 298 K) is reported as a function of the $TiO_2$ loading in Fig. 9. Surface coverage has been expressed as molecules over square nanometer to give a direct idea of the actual density of water molecules on the material surface considering the variation of materials specific surface area. The four isobars have similar shape and show that: (i) as expected $\sigma_{H2O}$ progressively increases by rising $p_{H2O}$, and (ii) the water uptake on the eight materials is rather different: for

instance the surface coverage of the T_10 sample is 2-2.6 times higher than the pure silica sample at all $p_{H2O}$. As a general tendency, for samples with a $TiO_2$ loading ≤ 10 % the surface coverage progressively increases by increasing the $TiO_2$ concentration. Indeed, small fluctuations can be observed in this trend, being the $\sigma_{H2O}$ of T_0.5 slightly smaller than that of T_0.0 and being $\sigma_{H2O}$ of T_1.0 slightly smaller than T_2.0 in all the isobars. On the contrary, there is a clear decline of surface coverage at a $TiO_2$ loading between 10 % and 20 %, and the T_33 sample shows $\sigma_{H2O}$ values 10-20% smaller than T_20.

### 3.5 Water adsorption: differential heat of adsorption

In order to determine the energy and the energy distribution of the water adsorption sites, the molar adsorption heat ($q_{ads}$) evolved for each dose of water contacted with the sample surface was calculated from the data in Fig. 6 by the following equation $q_{ads} = \Delta q_{ads}/\Delta N_{ads}$ Hence, $q_{ads}$ was plotted as a function of $\sigma_{H2O}$ for each material analyzed in this study. Two different behaviors were observed. In the case of T_0.0 and T_0.5 no significant changes were measured in $q_{ads}$ at different $\sigma_{H2O}$, as typical for homogenous surfaces. On the contrary, the other samples showed the characteristic behavior of heterogeneous surfaces, involving various reversible interactions of different energy. The curves of $q_{ads}$ vs $\sigma_{H2O}$ of the samples T_0.0, T_10, and T_20 are shown in Fig. 10 as illustrative examples. In the case of the T_0.0, an average $q_{ads}$ of 49 ± 1 kJ $mol^{-1}$ has been measured over an interval of $\sigma_{H2O}$ between 0.2 and 1.7 (molecules $nm^{-2}$). On the contrary, the first water molecules interacting with the surface of T_10 evolve an energy higher than 160 kJ $mol^{-1}$, while further water molecules are physisorbed with a less strong interaction, reaching a plateau of energy at about 69 ± 3 kJ $mol^{-1}$ for $\sigma_{H2O}$ > 2

(molecules $nm^{-2}$), i.e. always higher than that measured on Ti_0.0 sample and always higher than the latent heat of water condensation. The data concerning T_20 have a trend similar to T_10; but in this case lower energies were released at low $\sigma_{H2O}$, and a plateau energy of 76 ± 2 kJ $mol^{-1}$ was measured for a surface coverage higher than 1.5 (molecules $nm^{-2}$). In order to compare the different materials, the experimental points of the samples with a $TiO_2$ loading ≥ 1% were fitted with a simple exponential decay equation:

$$q_{ads}(\sigma) = \Delta q \cdot exp(-\sigma/\sigma_c) + q_{\#} \quad (1).$$

This method allowed determining three parameters, namely the decay constant $\sigma_c$, the offset $q_{\#}$, corresponding to the heat released by the physisorbed water molecules at high coverage, and the amplitude $\Delta q$, which is the difference between the heat of adsorption at zero coverage ($q_0$) and $q_{\#}$:

$$\Delta q = q_0 - q_{\#} \quad (2).$$

The values of $\sigma_c$ were smaller than 0.84 water molecules $nm^{-2}$ for all the samples, indicating that a steady $q_{\#}$ value is reached at relatively low coverage for all the materials presented in this study.

Fig. 11 shows the $q_{\#}$, $q_0$, and $\Delta q$ values as functions of the $TiO_2$ loading for the all the materials reported in this study. $q_{\#}$ represents the interaction of physisorbed water molecules just before multilayer formation, and thus it can be used as parameter to

determine the hydrophilicity of the material surface [45-47] In the case of T_0.0 and T_0.5, $q_{\#}$ is considered as the average of $q_{ads}$ over all the $\sigma_{H2O}$ range, because for these two materials the heat of adsorption was found to be independent of the surface coverage. All the $q_{\#}$ values reported in this study are larger than the latent heat of liquefaction of water (44 kJ mol$^{-1}$), indicating that all the samples are hydrophilic. Moreover, a clear trend is observed showing a gradual increase of interaction strength from T_0.0 (49 ± 1 kJ mol$^{-1}$) to T_33 (90 ± 5 kJ mol$^{-1}$).

$\Delta q$ represents the difference on interaction energy for water molecules adsorbed at zero coverage and at a high surface coverage, thus it can be used as a measure of the energy difference for the water adsorption sites. As we already discussed $\Delta q$ is ~ 0 kJ mol$^{-1}$ for T_0.0 and T_0.5. On the contrary, by considering the samples with a higher $TiO_2$ loading, it can be observed that $\Delta q$ increase from 24 ± 4 kJ mol$^{-1}$ for T_1.0 to 121 ± 5 kJ mol$^{-1}$ for T_10 whereas decreases down to 75 ± 6 kJ mol$^{-1}$ and 55 ± 13 kJ mol$^{-1}$ for T_20 and T_33 respectively. Fig. 11 shows also the heat of water adsorption at zero coverage ($q_0$) as calculated by Eq. 1 and sample T_10 presents the highest $q_0$ value, namely 190 ± 5 kJ mol$^{-1}$, together with the largest difference in the sites water adsorption energy.

### 3.6 Toluene adsorption

A complimentary technique was used to test the membrane materials towards the adsorption of a hydrophobic vapor, namely toluene, since the microcalorimetric apparatus is not suitable for such tests because hydrophobic vapors can dissolve in the grease of its glass vacuum line misrepresenting the real trend of materials adsorption. Thus, the amount of toluene adsorbed was measured on a stainless steel

microgravimetric equipment for selected samples. The results of this analysis are reported in Fig. 12 using the same format as in Fig. 9 to facilitate the comparison with water vapor adsorption isobars. At an equal partial pressure ($p_{0,toluene}$ = 39.5 mbar at 298 K), the samples show lower surface coverage for toluene than for water, confirming the hydrophilic character of the eight materials. At toluene partial pressure ($p/p°_{toluene}$) of 0.025 and 0.051 , $TiO_2$-containing samples show a higher toluene surface coverage ($\sigma_{toluene}$) than the pure silica samples. This result can be explained by considering that heterogeneous surfaces can allow adsorption of both water and hydrophobic vapors [31]. Nevertheless, at $p/p°_{toluene}$ of 0.127 and 0.152, T_10 shows the smallest $\sigma_{toluene}$, indicating that T_10 is the sample that has the highest affinity to water and the lowest affinity to toluene.

## 4. Discussion

### 4.1 Morphology

The first objective of this work was the synthesis of $TiO_2$-silica membrane materials with high specific surface area, high pore volume, small pores, narrow pore size distribution, and a good dispersion of $TiO_2$ in the siliceous matrix. This goal was achieved; however, *SSA* and $V_p$ were slightly different in the eight samples, due to the different behavior of Si(IV) and Ti(IV) species during the material synthesis and consolidation. XRD, TEM and $N_2$ gas-volumetric adsorption analyses showed that the eight materials presented in this study are completely or in the largest part formed by an amorphous porous phase, which in some cases acts as binder of crystalline $TiO_2$ nanoparticles. At least two order of pores were detected in this amorphous matrix, namely intrinsic micropores and small mesopores formed by thermal removal of CTAB.

All samples showed specific surface area higher than 620 $m^2 g^{-1}$. Silica powders doped with a small amount of $TiO_2$ presented higher surface areas than the pure silica sample. This phenomenon has been already reported in literature [13] and in our opinion can be ascribed to the different reactivity of silicon and titanium alkoxide which can lead to the formation of different types of primary particles during synthesis and hence lead to the formation of a less efficiently packed oxidic structure. On the contrary, at a high $TiO_2$ loading a dense anatase phase is formed at the detriment of both *SSA* and $V_p$. The anatase phase can be observed by TEM for sample with $TiO_2$ loading ≥ 10 mol % and by XRD for samples with $TiO_2$ loading ≥ 20 mol %. These observations are well in agreement with previous studies, placing the upper limit for the solubility of $TiO_2$ in $SiO_2$ at about 15 mol% [48-51]. Despite these differences, all the samples have similar pore structure with mean pore size < 2 nm, and show the same amorphous nature of the matrix.

**4.2 Chemical Stability**

Stabilization of silica membrane materials by $TiO_2$ and other transition metal oxides has been investigated in the recent years by several authors, mostly in relation to hydrothermal densification [52]. Despite that, stabilization mechanisms have not completely revealed. Two main hypotheses have been presented. In the case of sol-gel derived $TiO_2$-containing membranes, it has been proposed that the stability improvement is due to the enhanced resistance of Ti–O–Si bonds to hydrolytic bond cleavage [53] and to the increased network connectivity, as evidenced by the increased glass transition temperatures [13]. A similar mechanism was proposed for $ZrO_2$ - and $Nb_2O_5$-doped membranes [13]. On the other hand, Acosta et al. [54] reported

experimental evidences that the high stability of Co-containing silica membranes is provided by $Co_3O_4$ nanocrystalites, opposing to silica mobility.

In this study, the chemical stability of $TiO_2$-containg silica membrane materials was investigated by solubility tests at pH 2 and in basic environment. Silica is known to be highly stable in the pH range between 2 to 8 and to be highly soluble in alkaline environment [55]. On the contrary, titania is much more stable than silica at basic pH, but its solubility at pH 2 is not negligible [56]. Therefore, the results in Fig. 6 and Fig. 7 are not surprising. At pH 11 and 13, the Ti/(Ti+Si) molar ratio in solution is smaller than the stoichiometric value for all the powders and the solubility was reduced by incorporation of $TiO_2$ in the silica matrix for the samples with a $TiO_2$ loading $\geq$ 2%. At $TiO_2$ laoding < 2 % , Ti is plausibly brought in solution together with the dissolved silica. At pH 2, the Ti/(Ti+Si) molar ratio in solution is higher than the stoichiometric values for most of the samples and the addition of $TiO_2$ caused a progressive increase in the powder solubility from sample T_00 to sample T_05. Then, the solubility decreased from sample T_10 to sample T_33, that is, in the samples where anatase crystallites were observed by TEM analysis. It should notice that the composition of the leached at pH 2 is the same for the three powders with the highest $TiO_2$ loading, suggesting that $TiO_2$ addition above 10 % lead to the formation of a second phase, which is converted to anatase by calcination.

### 4.3 Hydrophilicity and surface heterogeneity

The water adsorption data reported in this study indicate that hydrophilic sorption sites (e.g. surface titanol groups, Ti-OH) are introduces on the membrane material surface by $TiO_2$ presence. These sites can binds water molecules allowing higher

surface coverage (Fig.7). Nevertheless, the density of these sites decreases above a $TiO_2$ loading of 10-20% with a consequent decrease of water uptake for sample T_33. These results can be explained by considering that for $TiO_2$ loadings ≥ 10 % a phase separation is observed with the formation of $TiO_2$ anatase crystals presenting a less extended surface and a minor number of surface sites available for water adsorption. Thus, further addition of $Ti^{4+}$ ions will not increase the number of water sorption sites, i.e. the hydrophilicity of the system, but will increase the size and the concentration of anatase crystallites, which form a more dense network and decrease the material pore volume. Indeed, as shown by TEM pictures in Fig. 2d, a large amount of anatase crystals is well dispersed in the amorphous matrix of the samples prepared at a $TiO_2$ loading of 20 %, and 33 %. The concentration and the crystal size of the anatase phase are such to be detected by XRD analysis (Fig. 1).

Also the energy and the energy distribution of the water sorption sites are strongly affected by the titania presence. By considering the 44 kJ $mol^{-1}$ as threshold values for distinguishing hydrophobic from hydrophilic substances, the pure silica powder reported in this study (T_0.0) is slightly hydrophilic ($q_{\#}$ = 49 ± 1 kJ $mol^{-1}$), as expected for sol-gel derived silica calcined at a moderated temperature [46-48]. The addition of titania increases the hydrophilicity of the membrane material with a monotonic increase of $q_{\#}$ with the titania loading (Fig. 9). This result can be explained by considering hydrophilicity as a result of the ionic character of the oxidic network [47,48], being silica a covalent non-metal oxide and titania an ionic metal oxide.

On the contrary, the trends of $q_0$ and $\Delta q$ are not monotonic, showing a maximum for T_10. In this respect, it should be considered that the water affinity of $TiO_2$-based materials, and in general their surface reactivity, is strongly dependent on their

polymorphism [33,34]. For instance significant differences in $q_0$ have been already reported between the anatase and rutile phases [57] In this study the samples prepared with $TiO_2$ loading < 5% were observed to be amorphous and highly homogeneous. For these samples, an increase in $Ti^{4+}$ concentration correspond to a sharp increase of $q_0$ and thus of $\Delta q$. Formation of a crystalline anatase phase is observed for $TiO_2$ loading between 5 and 10 %. After the new phase is formed, a further increase in $TiO_2$ concentration corresponds to a decrease of both $q_0$ and thus of $\Delta q$. Hence, the sample Ti_10 shows the highest number of sorption sites and also the sites with the highest energy, indicating this sample as the most hydrophilic material presented in this study. These results are confirmed by toluene adsorption measurements reported in Fig. 12, showing the lowest toluene adsorption at $p/p° = 0.152$ for T_10.

## 5. Conclusions

In this paper we reported experimental evidences that hydrophilicity of silica-based materials can be tuned by titania doping. Eight materials were synthetized and characterized by means of XRD, TEM and nitrogen sorption analyses. The affinity of these materials to water was directly investigated by measuring the differential heat of adsorption of water at low steam relative pressures. In general, the data reported in Fig. 7-10 clearly indicate that the materials considered in this study are hydrophilic and that their hydrophilicity is increased by the introduction of $TiO_2$ in the amorphous siliceous matrix. However, the formation of a dense anatase phase appears to have a negative influence on the surface density and energy distribution of the water adsorption sites, making the sample prepared at a $TiO_2$ loading of 10% the most hydrophilic, as confirmed by its limited affinity to toluene. The results presented in this study are

highly valuable for the design of hybrid materials useful for molecular separation processes, e.g. membranes and adsorbing systems, and the procedure applied to evaluate the surface behaviors of the materials can constitute a good approach to determine *a priori* the field of applicability and the target of a filtration setup.

## Acknowledgments

This work was realized with the contribution of the Marie Sklodowska-Curie Research and Innovation Staff Exchange project funded by the European Commission H2020-MSCA-RISE-2014 within the framework of the research project Mat4Treat (Project number: 645551).

## References

[1] R.K. Joshi, P. Carbone, F.C. Wang, V.G. Kravets, Y. Su, I.V. Grigorieva, H.A. Wu, A.K. Geim, R.R. Nair, Science 343 (2014) 752-754.

[2] M.M. Khin, A S. Nair, V.J. Babu, V. Jagadeesh, R. Murugan, R. Rajendiran, S. Ramakrishna, Energy Environ. Sci. 5 (2012) 8075-8109.

[3] L.M. Ortega, R. Lebrun, J.F. Blais, R. Hausler, Desalination 227 (2012) 204-216.

[4] S.P. Sun, T.A.; Hatton, S. Y. Chan, T. S. Chung, J. Membr.Sci. 401 (2012) 152-162.

[5] S. Sanches, A. Penetra, A. Rodrigues, E. Ferreira, V.V. Cardoso, M J. Benoliel, M.T. Barreto Crespo, V.J. Pereira, J.G. Crespo, Sep. Purif. Technol. 94 (2012) 44–53.

[6] K.V. Plakas, A. J. Karabelas, Desalination 287 (2012) 255-265.

[7] R.M. de Vos, H. Verweij, Science 279 (1998) 1710-1711.

[8] S. R. Chowdhury, A.M. Peters, D.H.A. Blank, J.E. ten Elshof, J. Membr.Sci. 279 (2006) 276-281.

[9] V. Boffa, J.E. ten Elshof, D.H.A. Blank, Microporous Mesoporous Mater. 100 (2007) 173–182.

[10] H.L. Castricum, A. Sah, R. Kreiter, D.H.A. Blank, J.F. Vente, J.E. ten Elshof, Chem. Comm. (2008) 1103-1105.

[11] H.L. Castricum, R. Kreiter, H.M. van Veen, D.H.A. Blank, J.F. Vente, J.E. ten Elshof, J. Membr. Sci. 324 (2008)111-118.

[12] G. G. Paradis, D. P. Shanahan, R. Kreiter, H. M. van Veen, H. L.Castricum, A. Nijmeijer, J. F. Vente, J Membr. Sci. 428 (2013) 157-162.

[13] V. Boffa, G, Magnacca, L. Bjerg Jørgensen, A. Wehner, A. Dörnhöfer, Y. Yue, Microporous Mesoporous Mater. 179 (2013) 242-249.

[14] A. Farsi, O. De Bartolis, G. Magnacca, P. K. Kristensen, M. L. Christensen, V. Boffa, in preparation.

[15] Q. Wei, Y.L. Wang, Z.R. Nie, C.X. Yu, Q.Y. Li , J.X. Zou, C.J. Li, Microporous Mesoporous Mater. 111 (2008) 97-103.

[16] K.C. McCarley, J. Douglas Way, Sep. Purification Technol. 25 (2001) 195–210.

[17] R.P. Singh, J.D. Waya, S.F. Dec, J.Membr.Sci. 259 (2005) 34–46.

[18] G.G. Paradis, R.Kreiter, M.M.A. van Tuel, A. Nijmeijer, J.F. Vente, J.Mater.Chem. 22 (2012) 7258 – 7264.

[19] V. Boffa, Fabrication of ultramicroporous silica membranes for pervaporation and gas-separation, in: B. Pignataro (Ed.), Molecules at Work, Wiley-VCH, 2012, pp.177-205.

[20] K. Yoshida, Y. Hirano, H. Fujii, T. Tsuru, M. Asaeda, J.Chem.Eng.Jap. 34 (2001) 523-530.

[21] M. Asaeda, Y. Sakou, J.H. Yang, K. Shimasaki, J.Membr.Sci. 209 (2002) 163-175.

[22] M. Kenezhashi, M. Asaeda, J.Chem.Eng.Jap. 14 (2005) 908-912.

[23] V. Boffa, D.H.A. Blank, J.E. ten Elshof, J.Membr.Sci. 319 (2008) 256-263.

[24] S. Battersby, T. Tasaki, S. Smart, B. Ladewig, S.M. Liu, M.C. Duke, V. Rudolph, J.C.D. da Costa, Sep.Purif.Technol. 329 (2009) 299-305.

[25] K. Brands, S. Uhlmann, M. Bram, J.C.D da Costa, J.Membr.Sci. 359 (2010) 110-114.

[26] S. Khanmohammadi, E. Taheri-Nassaj, Ceram.Intern. 40 (2014) 9403-9411

[27] V. Boffa, J.E. ten Elshof, A.V Petukhov, D.H.A. Blank, ChemSusChem 1 (2008) 437-443.

[28] H. Qi, H.R. Chen, L. Li, G.Z. Zhu, N.P. Xu, J.Membr.Sci. 421-422 (2012) 190-200.

[29] M. Kanezhashi, M. Asaeda, J.Membr.Sci. 271 (2006) 86-93.

[30] B. Fubini, Thermochim. Acta 135 (1988) 19-29.

[31] A. Cauvel, D. Brunel, F. Di Renzo, E. Garrone, B. Fubini, Langmuir 13 (1997) 2773-2778.

[32] B. Bonelli, B. Onida, J. D. Chen, A. Galarneau, F. Di Renzo, F. Fajula, B. Fubini, E. Garrone, Microporous Mesoporous Mater. 87 (2006) 170-176.

[33] J.W. Drazin, R.H.R. Castro, J. Phys. Chem. C 118 (2014) 10131−10142.

[34] V. Bolis, A. Cavenago, B. Fubini, Langmuir 13 (1997) 895-902.

[35] S. Brunauer, P.H. Emmett, E. Teller, J. Am. Chem. Soc. 60 (1938) 309-319.

[36] J.P. Olivier, J.Porous Mater. 2 (1995) 9-17.

[37] P. Baltazar, V.H. Lara, G. Córdoba, R. Arroyo, J.Sol-Gel Sci.Techn. 37 (2006) 129–133.

[38] T.L. Chew, A.L. Ahmad, S. Bhatia, Adv. Colloid Interf. Sci., 153 (2010) 43–57.

[39] R. Garcia Juez, V. Boffa, D.H.A. Blank, J.E. ten Elshof, 2008, J. Membr. Sci., 323 (2008) 347–351.

[40] C. Sanchez, C. Boissiere, D. Grosso, C. Laberty, L. Nicole, Chem Mater. 20 (2008) 682-737.

[41] K.S.W. Sing, D.H. Everett, R.A.W. Haul, L. Moscow, R.A. Pierotti, J. Rouquerol, T. Siemieniewska, Pure Appl. Chem. 57 (1985) 603-619.

[42] H. L. Castricum, A. Sah, R. Kreiter, D.H.A. Blank, J.F. Vente, J.E. ten Elshof, J. Mater. Chem., 18 (2008) 2150–2158.

[43] J. Sekulic, M.W.J. Luiten, J.E. ten Elshof, N.E. Benes, K. Keizer, Desalination 148 (2002) 19-23.

[44] C. J. Brinker, G.W. Scherer (1990) Sol-gel science: the physics and chemistry of sol-gel processing, Academic Press, San Diego (CA), USA, pag. 104.

[45] V. Bolis, B. Fubini, L. Marchese, G. Martra, D. Costat, J.Chem.Soc.Faraday Trans. 87 (1991) 497-505.

[46] B. Fubini, V. Bolis, M. Bailes, F.S. Stone, Solid State Ionics 32–33 (1989) 258-272.

[47] V. Bolis, C. Busco, M. Ciarletta, C. Distasi, J. Erriquez, I. Fenoglio, S. Livraghi, S. Morel, J.Colloid Interface Sci. 369 (2012) 28–39.

[48] D. L. Evans, J. Non-Cryst. Solids, 52 (1982)115-128.

[49] R. B. Greegor, F. W. Lytle, D. R. Sandstrom, J. Wong and P. Schultz, J. Non-Cryst. Solids, 55 (1983) 27-43.

[50] D. M. Pickup, G. Mountjoy, G. W. Wallidge, R. Anderson, J. M. Cole, R. J. Newport, M. E. Smith, J. Mater. Chem., 9 (199) 1299-1305.

[51] G. Mountjoya, J. S. Rigdena, R. Andersona, G. W. Wallidgea, R. J. Newporta, M. E. Smitha, J. Mater. Res. 15 (2000) 1998-2005.

[52] V. Boffa, Fabrication of ultramicroporous silica membranes for pervaporation and gas-separation, in Molecules at Work (B. Pignataro ed.) Wiley (2012) 177-205.

[53] Y. Gu, S. T. Oyama, J. Membr. Sci., 345 (2009) 267–275.

[54] L. Liu, D.K. Wang, P. Kappen, D.L. Martens, S. Smart, J.C. Diniz da Costa, Phys. Chem. Chem. Phys., 17 (2015)19500-19506.

[55] R.K. Iler, The Chemistry of Silica, John Wiley and Sons, New York, 1979

[56] J. Schmidt, W. Vogelsberger, J. Solution Chem., 38 (2009) 1267–1282.

[57] U. Aschauer, Y. He, H. Cheng, S.-C. Li, U. Diebold, A. Selloni, J. Phys. Chem. C 114 (2010) 1278–1284.

Table 1. Composition of the reaction mixtures used for the synthesis of the $TiO_2$-silica membrane materials.

| **Sample name** | **$TiO_2$ loading** (mol%) | **Hydrolized TEOS** 1.5 M solution (mL) | **Dilution 1** Ethanol (g) | **Dopant** $Ti(butO)_4$ (g) | **Dilution 2** Butanol (g) | **Dilution 3** Ethanol (g) | **Surfactant** CTAB (g) |
|---|---|---|---|---|---|---|---|
| T_0.0 | 0 | 133 | 57.85 | 0.00 | 40.00 | 25.00 | 7.00 |
| T_0.5 | 0.5 | 132 | 58.44 | 0.35 | 40.00 | 24.65 | 7.00 |
| T_1.0 | 1 | 132 | 59.02 | 0.70 | 40.00 | 24.30 | 7.00 |
| T_2.0 | 2 | 130 | 60.19 | 1.40 | 40.00 | 23.60 | 7.00 |
| T_5.0 | 5 | 126 | 63.71 | 3.50 | 40.00 | 21.50 | 7.00 |
| T_10 | 10 | 120 | 69.57 | 7.01 | 40.00 | 17.99 | 7.00 |
| T_20 | 20 | 106 | 81.28 | 14.02 | 40.00 | 10.98 | 7.00 |
| T_33 | 33 | 89 | 96.51 | 23.12 | 40.00 | 1.88 | 7.00 |

## Figure Captions

Fig. 1. XRD patterns of the TiO2-silica powders. The arrows indicates the peaks typical of the anatase phase, visible in the sample T_33.

Fig. 2. TEM pictures of the sample T_0.0 (a), T_5.0 (b), T_10 (c), and T_20 (d). White lines in section (c) stress fringe patterns of the anatase TiO2 nanocrystals. A detailed description of the micrographs is given in the text (section 3.2).

Fig. 3. Nitrogen gas-volumetric sorption isotherms of the eight materials presented in this study.

Fig. 4. BET specific surface area (*SSA*) and DFT specific pore volume (*VP*) as a function of the TiO2 loading for the materials presented in this study.

Fig. 5. DFT pore size distribution of the eight materials presented in this study.

Fig. 6. Silicon and titanium concentration in the leached solutions at pH 2, 11 and 13, as measured by ICP-OES analysis.

Fig. 7. Ti molar faction in the leached solutions at pH 2 and 13 as a function of the Ti molar fraction in the starting powder. The dashed line indicates stoichiometric leaching, i.e. the dissolved material has the same composition of the starting powder.

Fig. 8. Water-adsorption microcalorimetric data for T_10. Adsoprtion isotherm (section a) and calorimetric curves (section b) obtained at 298 K on sample outgassed *in vacuo* at 298 K.

Fig. 9. Surface coverage by water molecules ($\sigma_{H2O}$) for different steam relative pressures ($p/p°_{H2O}$) as a function of the TiO2 loading in the materials.

Fig. 10. Molar adsorption heat of water adsorption (*qads*) as a function of the surface coverage ($\sigma_{H2O}$) for the samples T_0.5, T_10 and T_20. The dashed lines indicate the best fit obtained for

T_10 and T_20 data points. The dotted line indicates the average of the *qads* values measured for T_0.0.

Fig. 11. Molar heat of water adsorption at zero coverage (*q0*), at high surface coverage ($q_{\#}$), and their difference ($\Delta q$), as a function of the TiO2 loading in the material.

Fig. 12. Surface coverage by toluene molecules ($\sigma_{toluene}$) for different toluene relative pressures ($p/p°_{toluene}$) as a function of the TiO2 loading in the material.

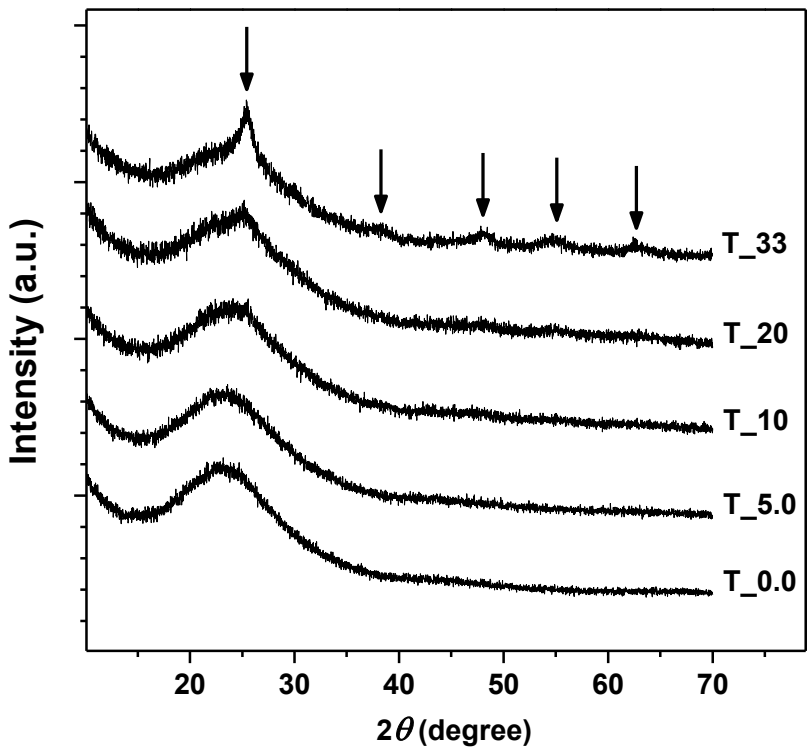


Fig. 1. XRD patterns of the $TiO_2$-silica powders. The arrows indicates the peaks typical of the anatase phase, visible in the sample T_33.

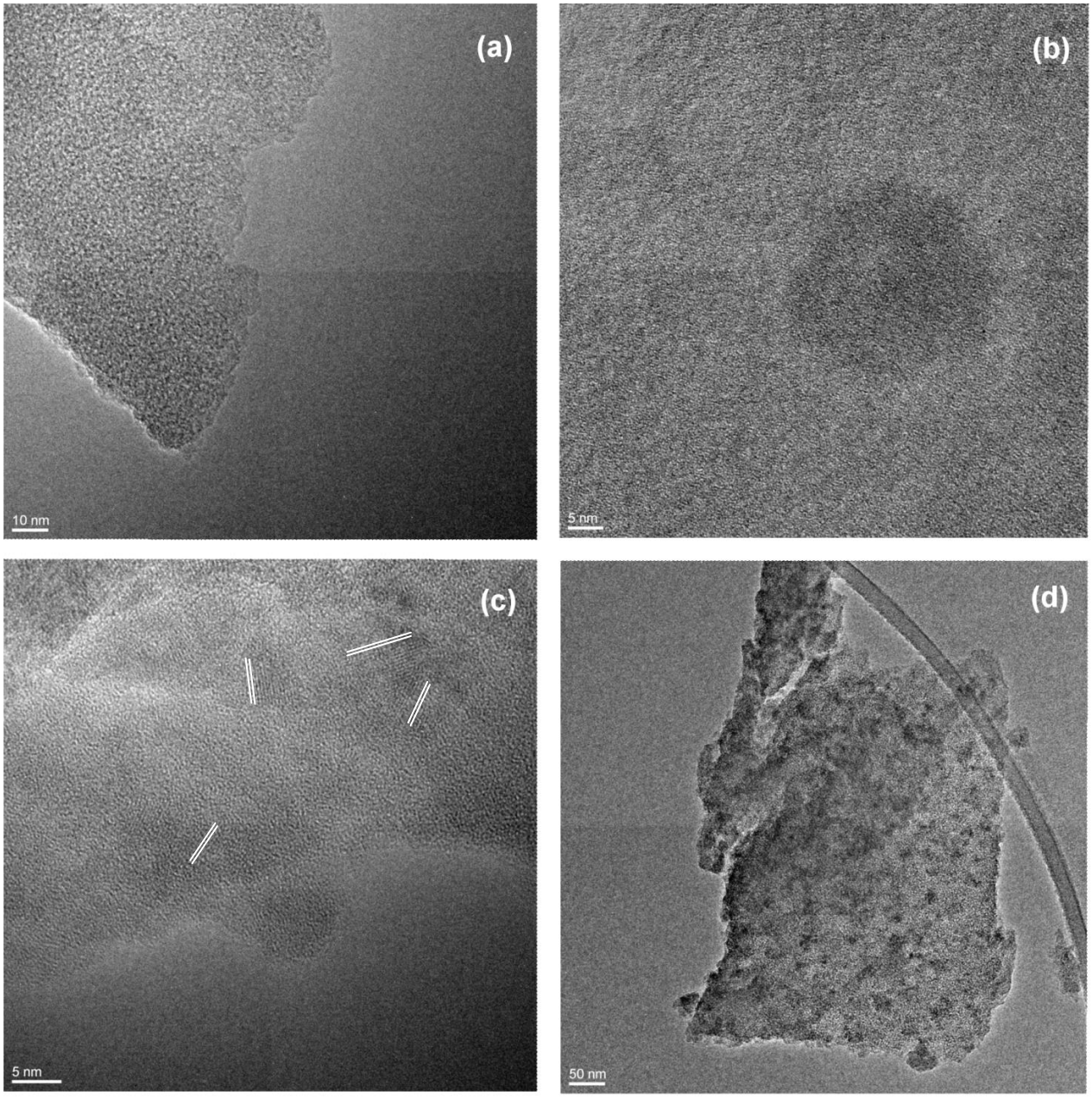


Fig. 2. TEM pictures of the sample T_0.0 (a), T_5.0 (b), T_10 (c), and T_20 (d). White lines in section (c) stress fringe patterns of the anatase $TiO_2$ nanocrystals. A detailed description of the micrographs is given in the text (section 3.2).

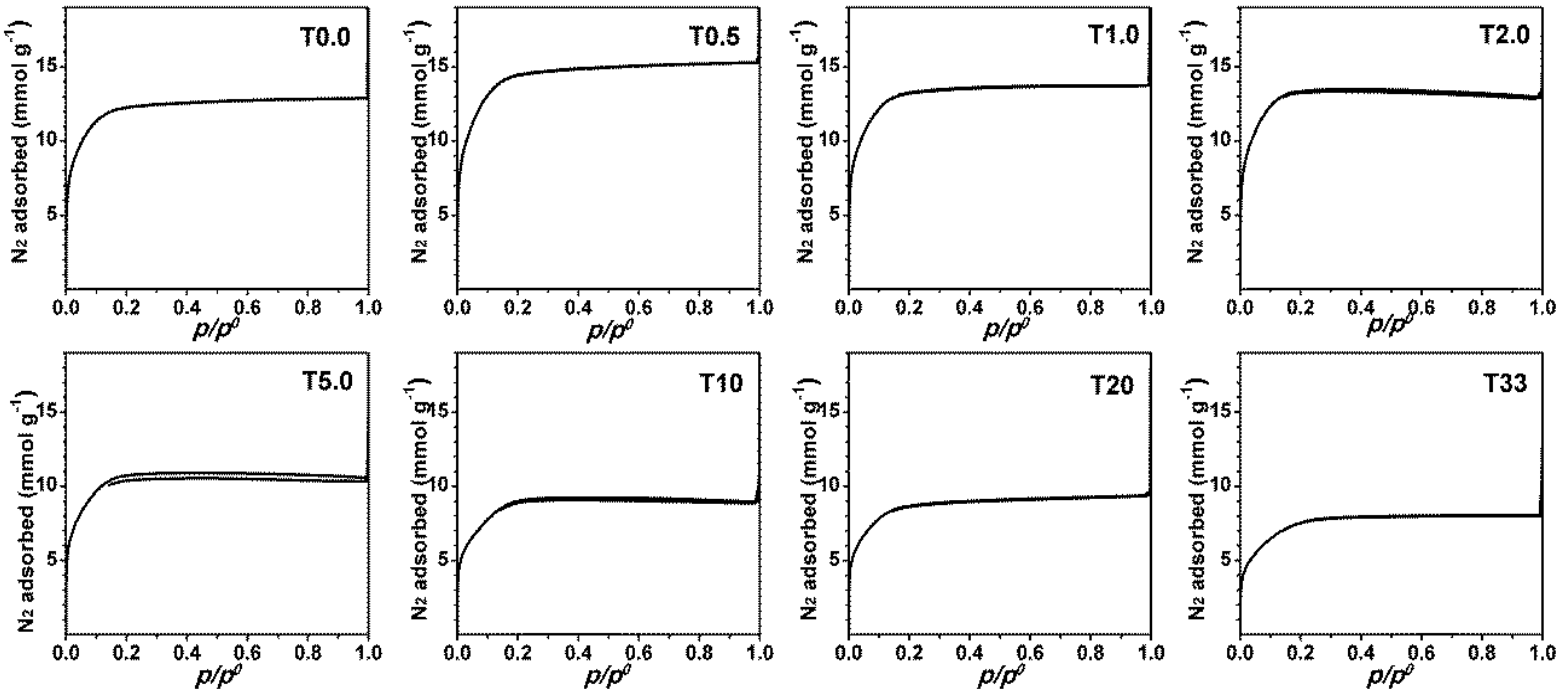


Fig. 3. Nitrogen gas-volumetric sorption isotherms of the eight materials presented in this study.

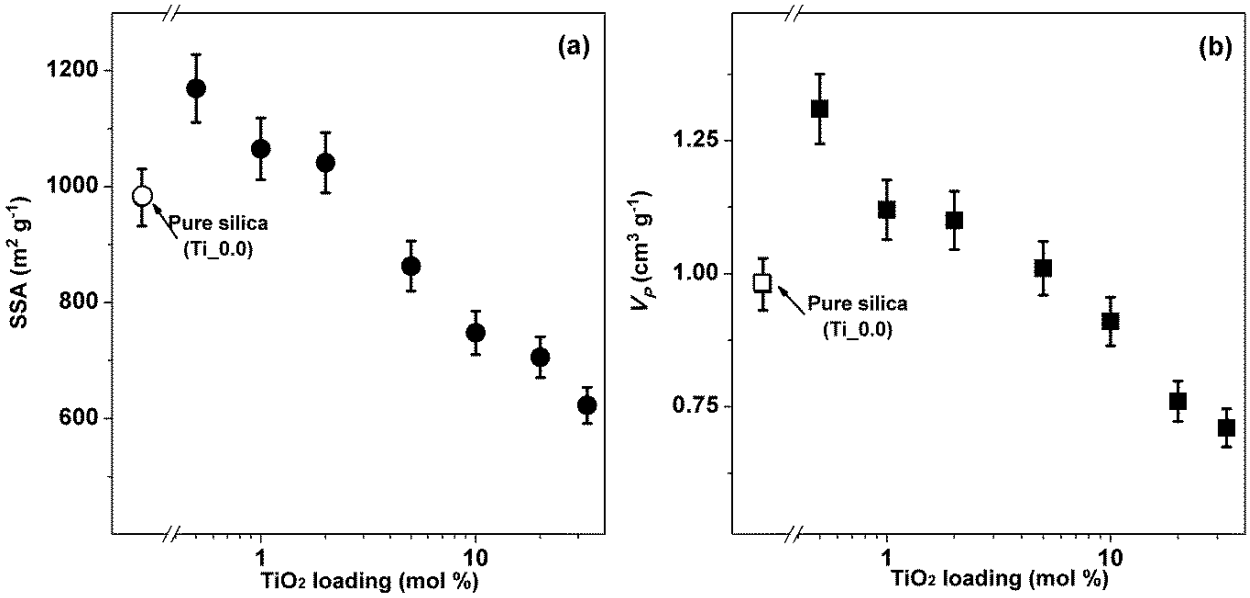


Fig. 4. BET specific surface area (*SSA*) and DFT specific pore volume ($V_P$) as a function of the $TiO_2$ loading for the materials presented in this study.

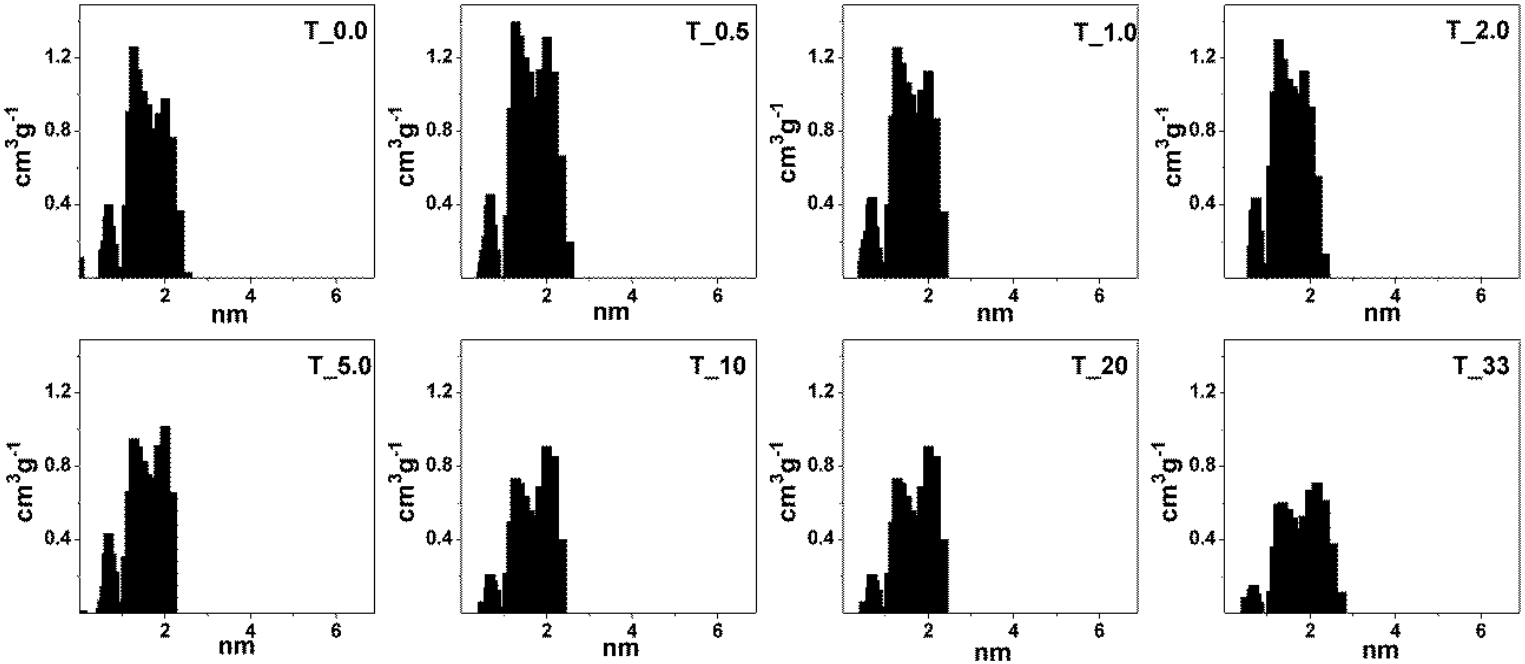


Fig. 5. DFT pore size distribution of the eight materials presented in this study.

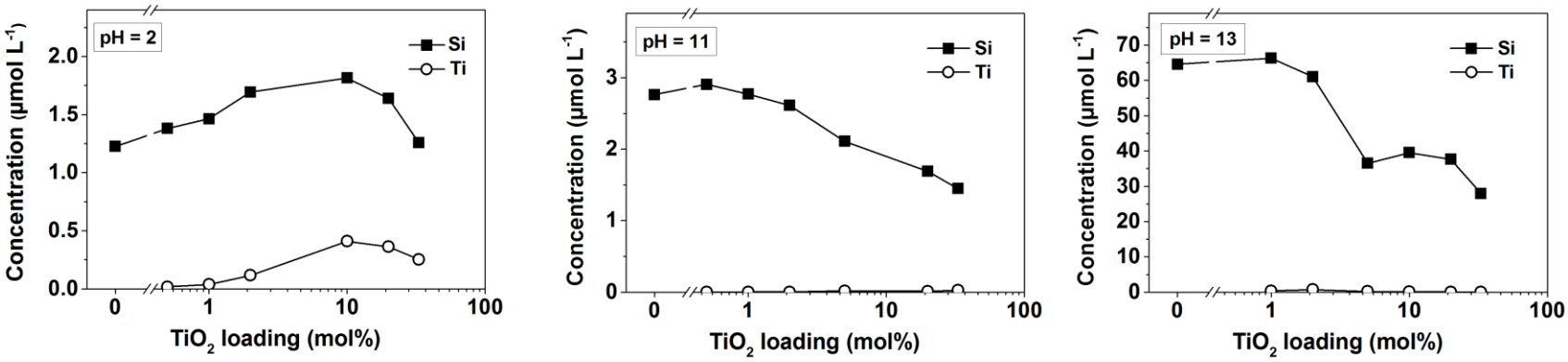


Fig. 6. Silicon and titanium concentration in the leached solutions at pH 2, 11 and 13, as measured by ICP-OES analysis.

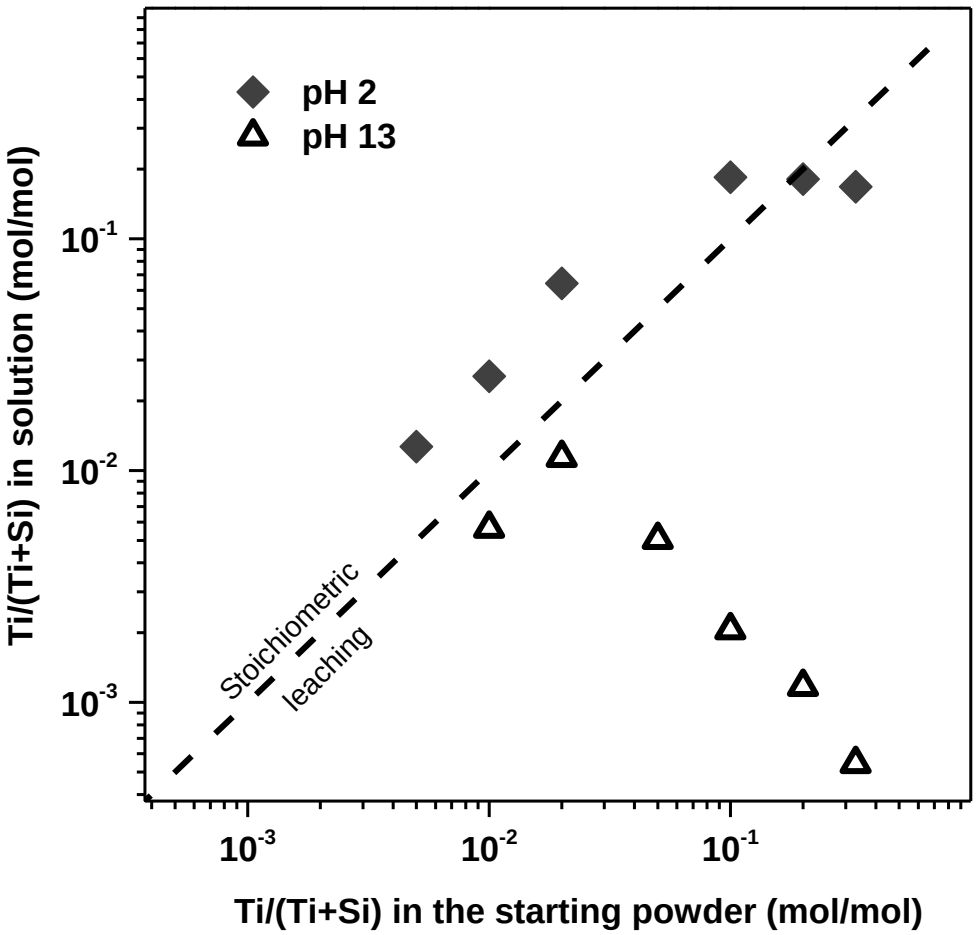


Fig. 7. Ti molar faction in the leached solutions at pH 2 and 13 as a function of the Ti molar fraction in the starting powder. The dashed line indicates stoichiometric leaching, i.e. the dissolved material has the same composition of the starting powder.

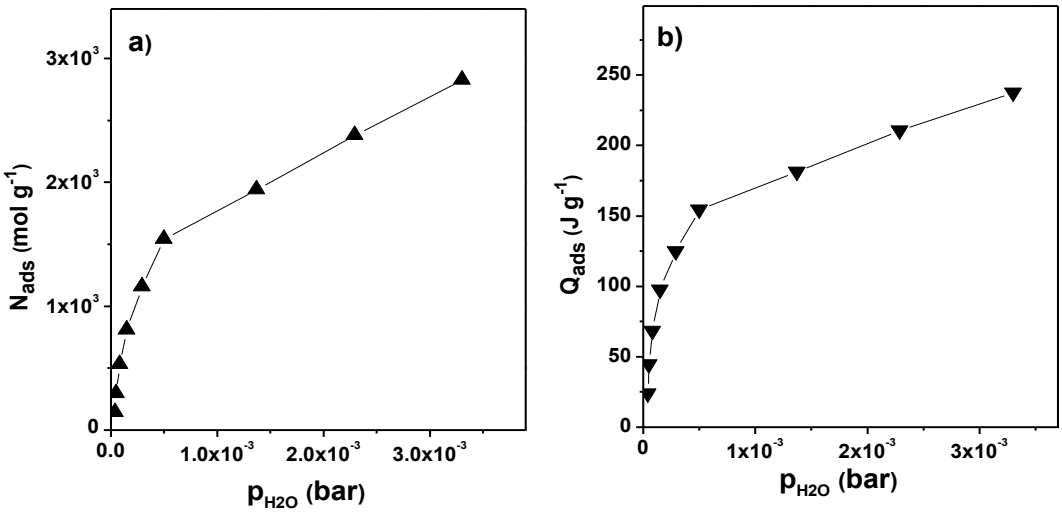


Fig. 8. Water-adsorption microcalorimetric data for T_10. Adsoprtion isotherm (section a) and calorimetric curves (section b) obtained at 298 K on sample outgassed *in vacuo* at 298 K.

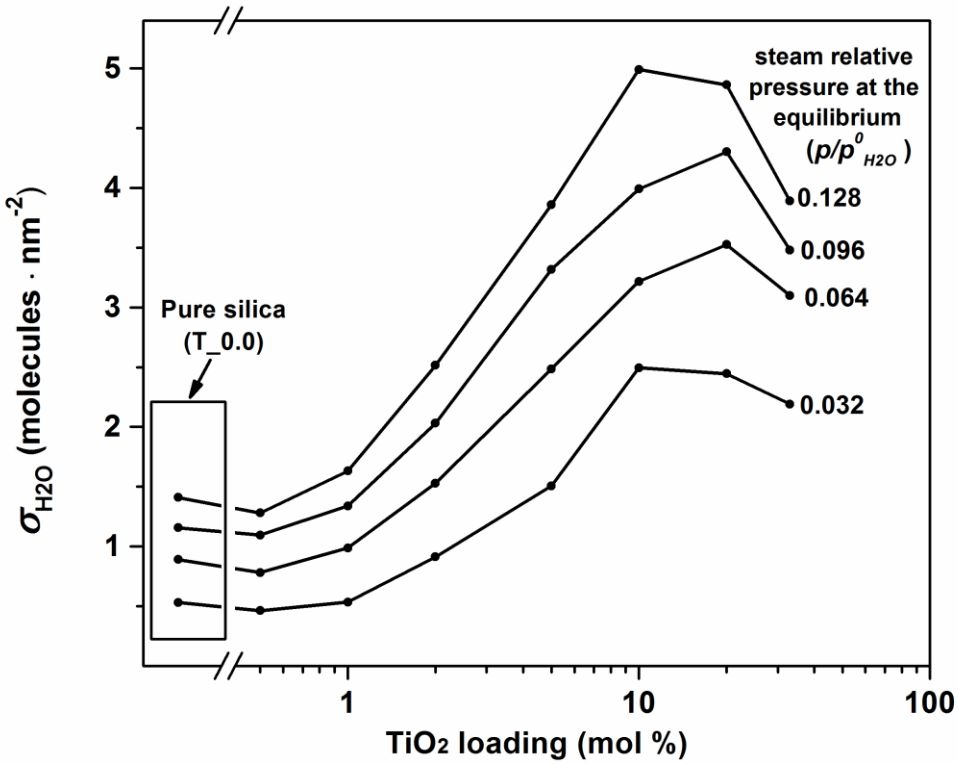


Fig. 9. Surface coverage by water molecules ($\sigma_{H2O}$) for different steam relative pressures ($p/p°_{H2O}$) as a function of the $TiO_2$ loading in the materials.

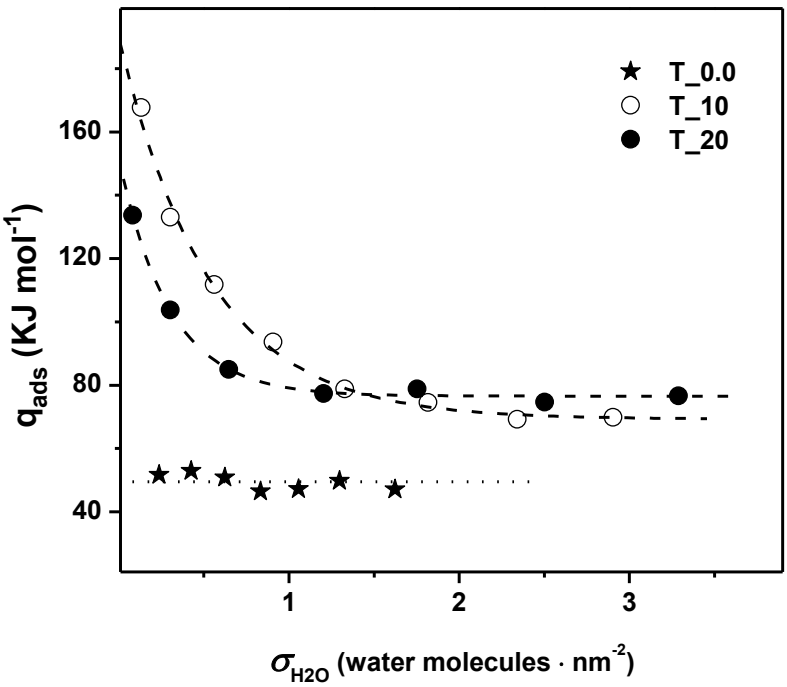


Fig. 10. Molar adsorption heat of water adsorption ($q_{ads}$) as a function of the surface coverage ($\sigma_{H2O}$) for the samples T_0.5, T_10 and T_20. The dashed lines indicate the best fit obtained for T_10 and T_20 data points. The dotted line indicates the average of the $q_{ads}$ values measured for T_0.0.

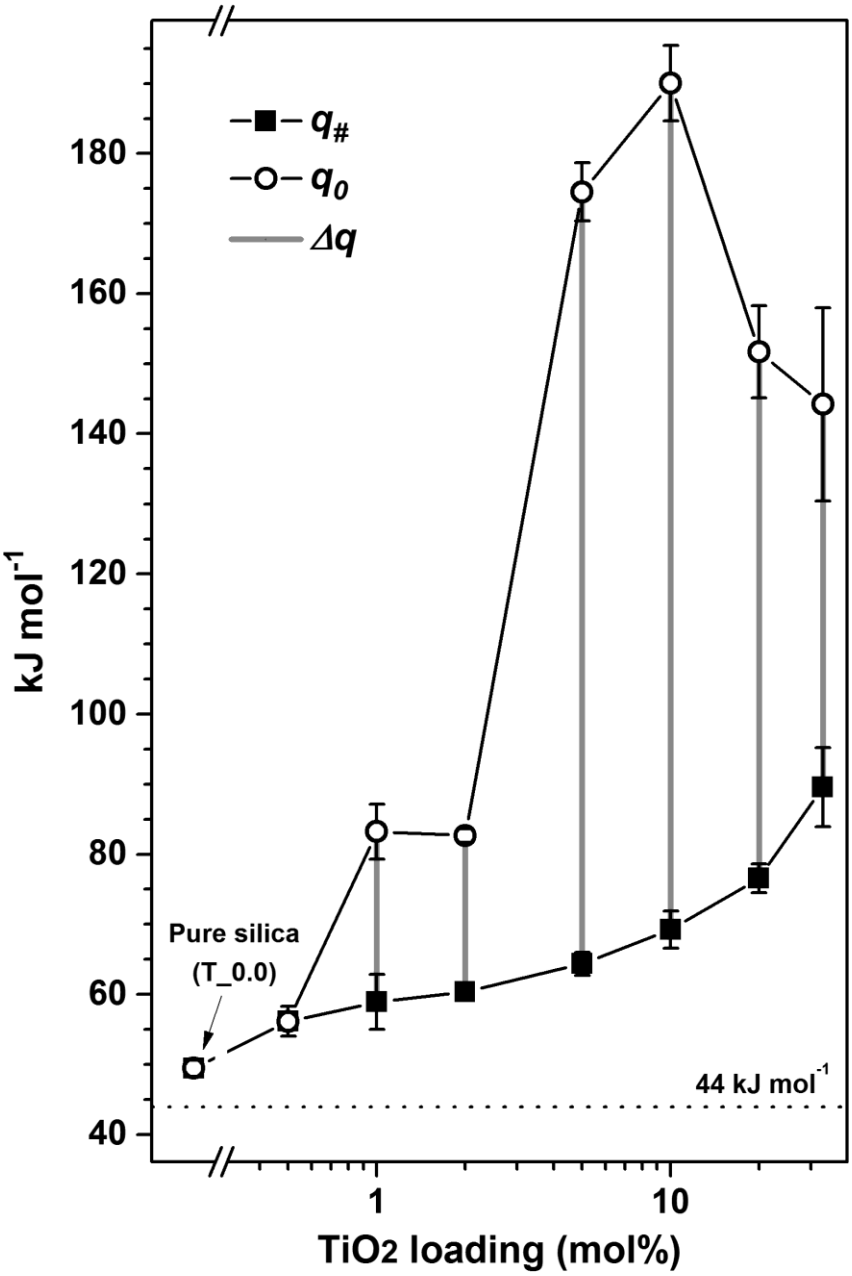


Fig. 11. Molar heat of water adsorption at zero coverage ($q_0$), at high surface coverage ($q_{\#}$), and their difference ($\Delta q$), as a function of the $TiO_2$ loading in the material.

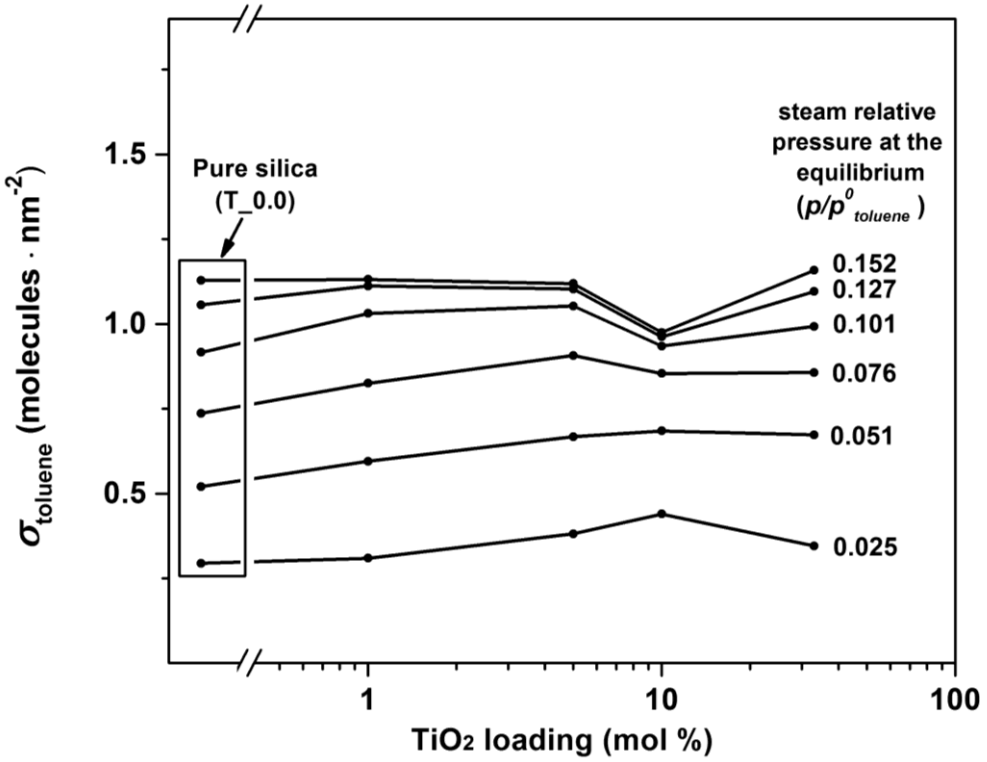


Fig. 12. Surface coverage by toluene molecules ($\sigma_{toluene}$) for different toluene relative pressures ($p/p°_{toluene}$) as a function of the $TiO_2$ loading in the material.